Experimental Characterization of the Heat Transfer in a latent Direct Contact Thermal Energy Storage with One Nozzle in Labor Scale

STEFAN KRIMMEL[1,2], ANASTASIA STAMATIOU[1,*], JÖRG WORLITSCHEK[1], HEIMO WALTER[2]
[1]Competence Center Thermal Energy Storage
[1]University of Applied Science Lucerne
[1]Technikumstrasse 21, 6048 Horw
[1]SWITZERLAND
[2]Institut of Energy Systems and Thermodynamic
[2]Technical University Vienna
[2]Getreidemarkt 9/T302, 1060 Vienna
[2]AUSTRIA

stefan.krimmel@hslu.ch [1]http://www.hslu.ch/tes [2]http://www.iet.tuwien.ac.at [*]corresponding author

Abstract: Latent direct contact thermal energy storage presents a promising way of storing thermal energy within a compact unit at high charging and discharging levels of power. On the one hand, the unconventional technique of heat transfer for storing energy depends essentially on the design and the material properties and on the other hand, there are a small number of investigation published in the known literature.
Based on basic experiments this paper discusses the fundamentals of the solidifying process by an upward droplet flow through the storage. Because of constant availability in high quality, water is chosen as storage material. The heat transfer fluid consists of thermal-oil with a low viscosity. The measurements includes the history of temperatures in addition to the mass flow of the heat transfer fluid out of seven experiment runs. Out of this data the thermal power is analyzed over the time and associated to the state of solidification. Simultaneously the findings of the experimental characterization contains the description of the power performance by dimensionless parameters as well as the discussion of the temperature distribution inside the storage tank.

Key-Words: Direct Contact Heat Exchange; Latent Thermal Energy Storage; Direct Contact Thermal Energy Storage; Heat Exchange; Temperature Distribution

1 Introduction

It exist a high accordance that thermal energy storages support the reduction of the energy demand in the domestic as well as in the industrial sector [1,2]. Latent thermal storages offer the potential to store the energy over a small temperature spread in a more compact way by the latent heat of the phase change than by the sensitive heat of one phase. This allowed installations with a low space and weight forces impact [3]. Despite the benefits, the power performance decrease in an early state which is often the challenge of the integration [4].
On the one hand, the PCM dominate the storage properties and could influence the installation costs significantly. The melting/solidification temperature, the phase change enthalpy and the grade of hazardous of the PCM are be given material properties [5–7]. On the other hand, the design of the heat exchanger and tank influence the power performance as well as installation costs and required space [8].
Finally, there exist two approaches to optimize the performance of latent thermal energy storages. Firstly material research to optimize or to develop new PCMs [9–11]. Secondly, and the focus of this research, the optimizing of the heat exchange and tank design [12,13].
Due to the low heat transfer by conduction of solid PCM (PCM_s) in comparison to the heat transfer by convection and conduction of liquid PCM (PCM_l) the thermal power decrease for an increasing grade of solidification in general [13]. A general approach to optimize the power performance is to increase the active surface for heat transfer for example by finned tubes. The next steps depend on the optimizing aim and could consist of the minimizing of the heat exchanger weight or the stabilization of the power performance over the time on a high level [14].
The strong dependency of the thermal power on the grade of solidification leads to oversized storages in respect to their volume and thermal capacity. This results in, inter alia, space requirement and installation costs of latent thermal energy storages [14].
This paper focuses on the description of the heat transfer mechanism in latent direct contact thermal energy storages (DCTESs) to optimize the power performance und to reduce the installation costs.

The existing literature about DCTESs shows experimental investigations of the storage performance, but the evaluation of the heat transfer mechanism was not in focus [15–17]. The numerical investigations also concentrate on the description of the performance curve without deriving correlations concerning the heat transfer [18–21].
In respect to the high calculation effort for simulation of two-phase flows, the literature about multi-phase flows presents mostly experimental results or numerical simulations of just a single detail [22–24]. The results of these investigations have a low transferability to the direct contact heat exchange in a DCTES. Here, the heat transfer mechanism differs from the documented process technologies in two essentially points:

1. phase change of one fluid during the flow,
2. only one fluid flows through.

In particular, the phase change between the liquid and solid state of the PCM during the storage process explains the low transferability. The particles and fixed structures of the PCM_s influences the already complex two-phase flow. Due to the PCM does not flow through the tank it initiate a backflow of the PCM_l what additionally influences the flow field.
It turns out that the description of the heat transfer in a DCTES is a field of research of its own right. In the absence of fundamental research, the publications concerning this topic are very specialized and refer to the particular project only. They are not systematically coordinated to investigate the flow and heat transfer mechanism.
To establish the missing fundamental research, this paper offers a first step for the characterization of the heat transfer rate by a plain experimental set-up. The experiments include investigations of a single HTF droplet flow (one nozzle) to describe the heat transfer rate and mechanism. Based on the experiments, evaluation methods as well as the experimental set-up for further studies are discussed.

2 Methodology

The design of the labor scale storage suggested a simple nozzle geometry as well as a simple tank geometry for the exclusionary of boundary effects. The research neglects the suitability of the T_{melt} of the PCM for an installation case. By what the PCM could selected for comparable test condition. Water has the big advantage that it is cheap, non-hazardous and in most laboratories available in high quality. Certainly, the anomaly of water must be discussed carefully when formulating generalized statements. The water was obtained from a demineralization cartridge in the laboratory with an electrical conductivity lower than 5 µS/cm. The synthetic HTF based on aliphatic hydrocarbons has a temperature operation range from -85°C to 230°C and the trading name is "Therminol® D12". The material properties of the PCM and the HTF near to the melting point are given for atmospheric pressure in *Table 1* with data from [25,26].
The calculation of characteristic values is based on the material properties of the HTF take account the linear approximations of the temperature dependency in Eq. (1) to (4) calculated from the data in [26] for the temperature range -15°C ≤ T ≥ 15°C.

Table 1: Material properties for the PCM (H_2O) [25] *and the HTF (Therminol® D12)* [26] *near to the melting point of the PCM at atmospheric pressure.*

Value		PCM_s	PCM_l	HTF
Reference temperature		<0°C	≥0°C	0°C
density ρ	[kg/m³]	916.8	999.9	776
dynamic viscosity η	[mPa s]	-	1.79	1.93
heat capacity c_p	[kJ/(kg K)]	2.072	4.228	2.025
heat conductivity λ	[W/(m K)]	2.256	0.565	0.113
Prandtl-Number Pr	[-]	-	13.41	34.57
purpoint	[°C]	-	-	-85
melting temperature T_{melt}	[°C]	0		-
fusion-enthalpy Δh_{latent}	[kJ/kg]	333.69		-

$$\rho_{HTF}(T) = 776 - 0.8045 \cdot T \left[\mathrm{kg/m^3}\right] \quad (1)$$

$$\eta_{HTF}(T) = 1.93 - 0.037 \cdot T \left[\mathrm{mPa \cdot s}\right] \quad (2)$$

$$c_{p,HTF}(T) = 2.0256 + 0.0041 \cdot T \left[\mathrm{kJ/(kg \cdot K)}\right] \quad (3)$$

$$\lambda_{HTF}(T) = 0.113 - 0.001 \cdot T \left[\mathrm{W/(m \cdot K)}\right] \quad (4)$$

The experiments include a variation of the mass flow of the HTF $\dot{m}_{HTF}$ between 40 and 140 kg/h through a single nozzle with a diameter (D_n) of 5 and 2 mm in a 12 l storage tank. The heat transfer is calculated based on the temperature and the mass flow measurements of the HTF.
Non-dimensional values characterize the heat transfer over the load state of the storage. The characteristic of the temperature distribution inside the tank, the outlet temperature and the heat transfer between the HTF-droplet flow over the time are be discussed on an exemplary experimental run.

2.1 Experimental Set-Up

The experimental set-up is shown in Fig. 1, it consist primarily of the storage tank (a) which is connected from the outlet extraction (b) by steel pipes over a

frequency controlled pump (d) and a thermostat unit (f) to the nozzle plate (h) as inlet for the droplet flow (i). The main components are be given in Table 2.
By the magnetic valves V_1 to V_3 the flow could adjust into three circuits:

C1: open valves: V_1, V_3 storage tank
C2: open valves: V_2 by-pass
C3: open valves: V_1, V_2, V_3 storage tank and by-pass

By the manual valve V_4 the HTF level in the storage tank is controllable.

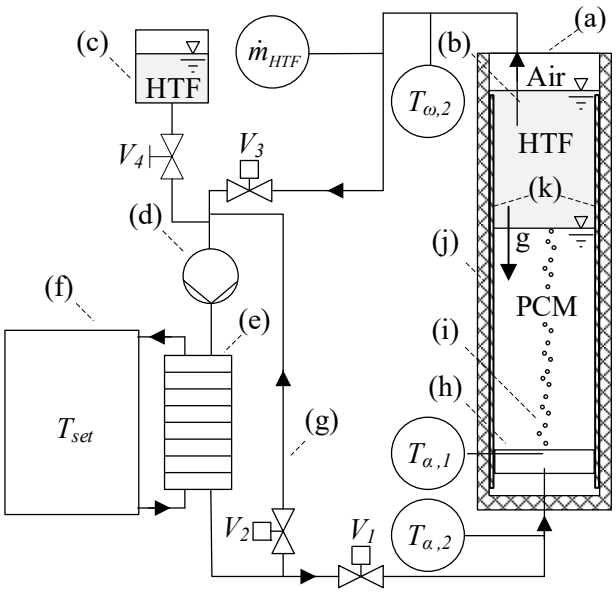

Figure 1: Flow chart of experimental set-up. (a) Storage tank; (b) outlet extraction; (c) expansion tank; (d) pump; (e) plate heat exchanger; (f) thermostat unit; (g) by-pass; (h) nozzle plate; (i) droplet flow, ascending against the gravity; (j) insolation; (k) plate LED strips.

Table 2: Manufacture and model number of the main extern manufactured components in the test rig.

Component	Manufacture	Model
(c) pump	Grundfos	CRE 5-4
(d) heat exchanger	Sweb	B12 NoP 60
(e) thermostat	Huber	Unistat 510

The storage tank has a rectangular basic shape with the dimension 200 x 78 mm (wide x depth) and a high of 800 mm. The front plate is made of triple isolated glass to allow optical observations and mounted of a carbon fiber back shell, which at the top is open to the ambient. The back shell is isolated with two layers of Armaflex HT 13-99/E. On the inner side of each sidewall a power controlled COB-LED plate is mounted to lighten the droplet flow.

While in standby situation without a HTF mass flow through the storage, there are two interfaces. One is between the PCM_l and the HTF, the second between the HTF and the air. Due to the densities (given in Table 1) of the fluids the PCM_l is in the lower part of the tank with HTF on the top which has the final interface to the ambient air.
The nozzle plate is made of PMMA to allow the optical observation of the flow inside the plate as well. The inlet tube (a) is 6 mm steel tube glued into the bottom plate and covered with a flow breaker (b). The nozzle (c) is a replaceable 3 mm thick PMMA quadratic plate (40 x 40 mm) with a borehole in the center as seen in the pictures of Fig. 2. The seal (d) is wide enough to close the space between the nozzle plate and the tank walls.

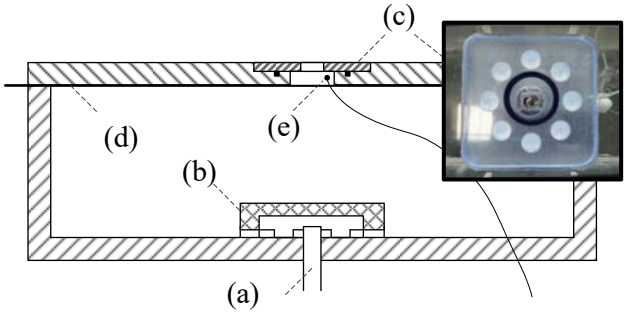

Figure 2: Simplified 2D-Cut of the nozzle plate with the main components numbered and a picture from the top view of the nozzle. Components: (a) inlet tube; (b) flow breaker; (c) nozzle; (d) seal; (e) thermocouple for $T_{\alpha,1}$.

2.2 Measurement Techniques

In the test rig there are integrated three temperature and one mass flow measurement integrated as seen in Fig. 1. Further, a mobile thermal measurement rack (MTMR) with 28 thermocouples (TCs) can be added into the tank to measure the temperature field, see Fig. 3. The TCs have a distance of s = 20 mm to the MTMR, 40 mm in the horizontal and 60 mm in the vertical direction. The measuring plane is central to the nozzle.
In the PCM layer are 7 TCs arranged in the vertical direction ($T_{PCM,i,j=3}$ with i = 1(bottom) … 7(interface)) and 12 TCs arranged at 3 levels in horizontal direction ($T_{PCM,i,j}$ with i=1,4,7; j = 1(left) … 5(right)). In the HTF layer are 4 TCs arranged in the vertical direction $T_{HTF,i,j=3}$ with i = 8(interface) … 11 (top)) and 4 TCs arranged in horizontal direction ($T_{HTF,i=10,j}$ with j = 1 (left) … 5 (right)). Obviously, the MTMR and the TCs will influence the

fluid dynamic behavior. Against this background, the temperature distribution was measured during the experiment runs 4_{III} and 4_{V} only.

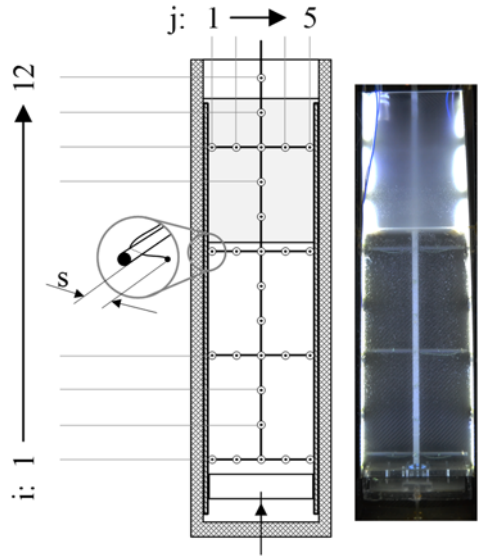

Figure 3: Mobile thermal measurement rack with 28 TCs to measure the temperature field in the storage. Left: drawing of the theoretical position with three horizontal line in the PCM and one in the HTF level. Right: Picture of the mobile temperature measurement rack in the tank without a HTF flow.

The properties of the thermal sensors are be given in *Table 3*. Calibration was done at two reference points, first in ice water at 0°C and second in air against a calibrated PT-100 at 21°C. Internal PT-100 sensors of the measurement transducer cards measured the cold junction temperature of the TCs. The relative error of the temperature sensors is determined with ±0.07 K, including the uncertainly due to the compensation of the cold junction an absolute error of ΔT_{error} = ±0.8 K has to be taken into account.

At the measurement point for $T_{\alpha,1}$ the TC is placed directly in the channel in front of the nozzle, see Fig. 1 and Fig. 2. The PT-100 sensors for the measurement points for $T_{\alpha,2}$ and $T_{\omega,2}$ are screwed with a T-piece into the 12 mm stainless steel tubes at the in- and outlet of the storage, see Fig. 1.

Table 3: Type and dimensions of the thermal sensors

Point	Type	Dimension
$T_{\alpha,1}$	TC K-Type	d = 0.3 mm, bare wire
$T_{\alpha,2}$ $T_{\omega,1}$ T_a	PT-100	l = 80 mm, d = 4 mm, stainless steel jacketed
$T_{fluid,i,j}$	TC K-Type	d = 0.3 mm, bare wire

For the measurement of the mass flow a coriolis flowmeter Promass 80F (Endress+Hauser) is used. The uncertainty of the mass flow is given with ±0.15% of the measured value.
The measurement transducer is the cDAQ9198 with the cards NI9216, NI9214, NI9212 and NI9213 from National Instruments. The time step of the data logger is set to 2 seconds.
For the optical documentation of the droplet flow and the phase change processes two cameras are be placed on a specified position in front of the optical access. One camera observes the whole area of the optical access and the other camera is be adjusted to the area over the nozzle plate. Every 2 seconds a picture is taken by each camera without being synchronized to each other or to the data logger.

2.3 Experimental Procedure

The experimental procedure for the characterization of the storage performance is standardized as seen in Fig. 4. It is subdivide into 6 periods:

I. pre-cooling,
II. temperature change of the thermostat,
III. solidifying by cooling down from 1 to -1°C,
IV. temperature change of the thermostat,
V. melting by heating from -1 to 1°C,
VI. overheating from 1°C to T_{set}.

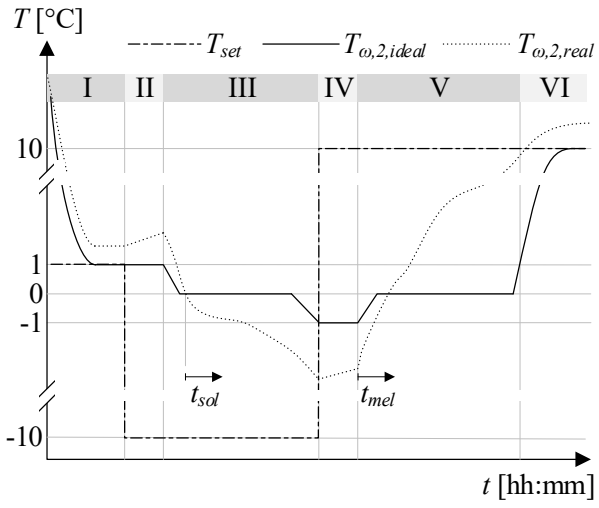

Figure 4: Scheme of the standardized experimental procedure with 6 periods of one storage cycle. $T_{\omega,2,ideal}$ would be the response answer of an ideal system to T_{set}. $T_{\omega,2,real}$ is an exemplary trend of the response from the measured response to T_{set}.

2.3.1 Pre-cooling (I)

During the first period of the procedure, the test rig reach the thermodynamically initial conditions. The valves open the flow circuit C3, see Fig. 1, and due to heat resistance and (negative) heat losses of the system the initial temperature of the storage is above the set temperature of T_{set} = 1°C at the thermostat. The pre-cooling is completed when $T_{\omega,2}$ is constant for a minimum of 5 minutes.

2.3.2 Temperature Change of the Thermostat (II and IV)

For each temperature change of the inlet temperature of the tank, the temperature of the oil in the thermostat and the temperatures of the HTF in the tubing have to change. During the periods II and IV the flow circuit C2 is active, see Fig. 1, and the periods are finished, if $T_{\omega,2}$ is constant for a minimum of 2 minutes. Due to (negative) heat losses, the temperature $T_{\omega,2}$ increase at the measurements point in the outlet tube.

2.3.3 Solidifying by Cooling Down from 1 to -1°C (III)

For an ideal system the period III represents primarily the solidification process. Respectively, the sensitive cooling of the PCM_l and PCM_s at the beginning and the end belong to the period as well. The time of the latent phase change can be identified the constant temperature $T_{\omega,2}$. The start time is defined by the first time point where $T_{\omega,2,real}$ fall below T_{melt}. Due to the missing of a plateau, the end of the solidification could not determined by the temperature chart. The optical observation shows that no experimental run reaches a state of complete solidified PCM.
During period III the valves activate the flow circuit C1, see Fig. 1.

2.3.4 Melting by Heating from -1 to 1°C (V)

At the beginning of period V the start temperature is identical with the temperature of the end of period III. From this start temperature, it is be heated up to 1°C including the melting of the PCM. For an ideal system, it is the inverse process of period III. Due to the real behavior in period III and the period IV the real starting temperature $T_{\omega,2,real}$ is lower and the PCM is not completely molten. The path of $T_{\omega,2,real}$ shows in general no tendency to a definite plateau, instead it increases in a wavy form. The beginning time stamp for the melting process of the PCM_s is the start of period V that is defined by switching from flow circuit C2 to C1. The end of the melting process is not clearly determinable.

2.3.5 Overheating from 1°C to T_{set} (VI)

The optional period VI is not part of the experimental investigation. It includes the period of an ideal system where the temperature $T_{\omega,2}$ rises above 1°C till it reaches a constant value above T_{set} or the flow of the HTF is shut down. In respect to the missing defined end of the period V for a real system, the beginning of period VI is in general undefined as well. However, after a sufficient period of time the system reach stationary operation point and due to (negative) heat losses $T_{\omega,2}$ is higher than T_{set} of the thermostat.

2.4 System Boundaries of Reference Systems

In general the definition of the nomenclature by storage investigation is based on storage temperatures above the ambient temperature. Against this background the direction of the heat flows in the following drawings are orientated for this case. For storage temperatures below the ambient, the losses became negative and the storage get an energy input out of the losses.

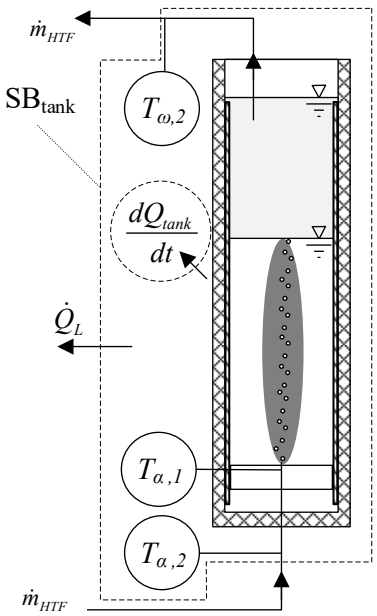

Figure 5: Definition of the system boundaries of the storage (SB_{tank}) and the interesting area of heat transfer in dark grey.

The system boundary of the storage tank (SB_{tank}) cuts the in- and outlet pipes of the storage at the measurement points for $T_{\alpha,2}$ and $T_{\omega,2}$. It include a single heat flow $\dot{Q}_L$ for the sum of heat losses as well

as one transient term for the energy change of the whole tank, see Fig. 5 and Eq. (6) and (7). By the SB_{tank} is the storage tank a black box for the analyses and the $\dot{Q}_L$ and the transferred energy from the HTF to the storage system could be determined, though it delivers no detailed information about the major heat flow during the multiphase flow, see Fig. 5.
However, the SB_{tank} is most common and most useful for an assessment or comparison of storage technologies. It characterizes the whole storage and can be measured by a low technical effort. With reference to Fig. 5 the adapted equation from the first law of thermodynamic is formulated for the transferred thermal energy by the HTF flow $\dot{H}_{storage}$ (9) and for the stored energy Q_{stored} (11).

$$\frac{dQ_{\text{tank}}}{dt} = \frac{dQ_{\text{HTF}}}{dt} + \frac{dQ_{\text{PCM}}}{dt} \tag{5}$$

with:

$$\frac{dQ_{HTF}}{dt} = m_{HTF} \cdot c_{p,HTF} \cdot \frac{d\overline{T}_{HTF}}{dt} \tag{6}$$

$$\begin{aligned}\frac{dQ_{PCM}}{dt} &= c_{p,PCM,s} \cdot m_{PCM,s}(t) \cdot \frac{d\overline{T}_{PCM,s}}{dt} + \\ &+ c_{p,PCM,l} \cdot m_{PCM,l}(t) \cdot \frac{d\overline{T}_{PCM,l}}{dt} + \\ &+ \frac{dm_{PCM,s}}{dt} \cdot \Delta h_{latent}\end{aligned} \tag{7}$$

with:

$$m_{PCM} = m_{PCM,s}(t) + m_{PCM,l}(t) \tag{8}$$

During the phase change processes of an ideal system is $\frac{dT_i}{dt} = 0$ in Eq. (6) and (7).

$$\dot{H}_{tank} = \frac{dQ_{tank}}{dt} + \dot{Q}_L \tag{9}$$

with:

$$\dot{H}_{tank} = \dot{m}_{HTF} \cdot c_{p,HTF} \left(\overline{T}_{HTF}\right)\left(T_{\omega,2} - T_{\alpha,2}\right) \tag{10}$$

$$Q_{tank} = \int \left(\frac{dQ_{tank}}{dt} - \dot{Q}_L \right) dt \tag{11}$$

For characterizing the heat transfer between the HTF and the PCM the storage tank is subdivided into 5 subsystems, see Fig. 6. Within this subdivision, the inlet boundary from the subsystem I and the outlet boundary from the subsystem IV are congruent with the counterparts from SB_{tank}. As well, the heat losses $\dot{Q}_L$ from the tank are equal to the sum of the heat losses from the subsystems, see Eq. (12).

$$\dot{Q}_L = \dot{Q}_{L\omega} + \dot{Q}_{LH} + \dot{Q}_{LP} + \dot{Q}_{LN} \tag{12}$$

System Boundary PCM
The closed system PCM consider the heat flow from the HTF droplet flow ($\dot{Q}_{HP}$) and the losses to the ambient ($\dot{Q}_{LP}$) as well as a transient term for the heat capacity of the PCM ($\dot{Q}_{PCM}$). The heat flows to the nozzle plate (System I) and over the interface on the top to the HTF (System III) are neglected.

System Boundary I
The open system I encloses the tube from the measurement point for $T_{\alpha,2}$ up to the nozzle by the measurement point for $T_{\alpha,1}$. Beside the enthalpy flow, it takes into account the heat losses $\dot{Q}_{LP}$ from the tube to the ambient and neglects the heat flows inside the storage.

System Boundary II
The open system II encloses the area by the sum of the HTF-droplets and represents the heat transfer according to the characterization of this paper.

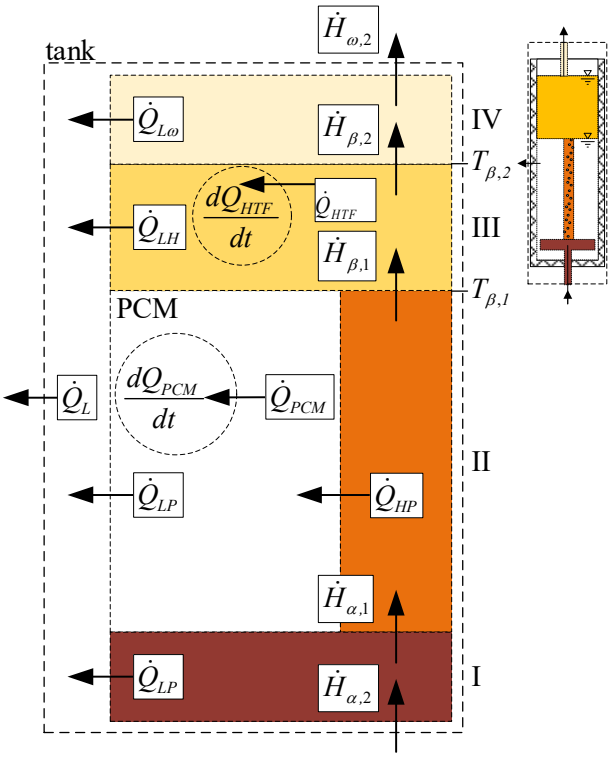

Figure 6: System boundaries of the storage tank.

System Boundary III
The open system III encloses the HTF layer above the PCM and includes a transient term for heat capacity of the HTF.

System Boundary IV
The open system IV encloses HTF in the extraction tube from the HTF surface up to the measurement point of $T_{\omega,2}$.

For the determination of the enthalpy flows in the subsystems the temperature at the boundaries β_1 and β_2 is necessary. With the given relationships of the energy and enthalpy flows in Fig. 6, the temperature $T_{\beta,1}$ is calculated backwards from the temperature $T_{\omega,2}$. This calculation will be deduced and verified in chapter 3.1.1.

2.5 Mathematical Description of Analysis

In order to characterize the heat transfer the heat effectivity Φ is a common value, which also is known as the operational characteristic of a heat exchanger (HEX), see Eq. (13). With respect to the constant temperature during the phase change of the storage, the maximal temperature difference is calculated due to T_{melt} and not due to the inlet temperature of the second fluid, see Eq. (14).

$$\Phi_{HEX} = \frac{T_{1,in} - T_{1,out}}{T_{1,in} - T_{2,in}} \quad \left(0 \le \Phi_{\mathrm{HEX}} \le 1\right) \tag{13}$$

Indices:
1 = fluid 1 (lower thermal capacity flow as fluid 2);
2 = fluid 2.

$$\Phi_{DCTES} = \frac{T_{HTF,in} - T_{HTF,out}}{T_{HTF,in} - T_{melt}} \quad \left(0 \le \Phi_{DCTES} \le 1\right) \tag{14}$$

Due to the transient characteristic of a storage process, Φ_{DCTES} is dependent upon state of load from the storage. The load takes the latent energy into account, which corresponds to the solidified mass of PCM and exclude a sensitive component. By that definition the state could be described with the solidification ratio Ψ_{DCTES}, see Eq. 15.

$$\Psi_{DCTES} = \frac{m_{PCM,s}}{m_{PCM}} \quad \left(0 \le \Psi_{DCTES} \le 1\right) \tag{15}$$

The total mass m_{PCM} is be given by the experimental set up and Eq. (16) calculate the mass of solidified PCM for the assumption of an ideal system in Eq. (7). If the assumption is not true and the sensitive heat of the PCM cannot be neglected, the whole Eq. (7) has to be used.

$$\dot{m}_{PCM,s} = \frac{\dot{Q}_{PCM}}{\Delta h_{latent}} \tag{16}$$

The stored energy by the phase change Q_{PCM} is be calculated by Eq. (17). If sensitive heat has to be considered, the Eq. (17) may not be allowed to use as well.

$$Q_{PCM} = \int_{t(T_{\alpha,1}=0°C)}^{t_{status}} \left(\dot{H}_{12}(t) - \dot{Q}_{LP}\left(\Delta T_{PCM,a}\right)\right) dt \tag{17}$$

with:

$$\Delta T_{PCM,a} = T_a - T_{PCM} \tag{18}$$

$$\dot{H}_{12} = \dot{m}_{HTF} \cdot c_{p,HTF} \cdot \left(T_{\beta,1}(t) - T_{\alpha,1}(t)\right) \tag{19}$$

with: in respect to the temperature range of the experiments and Eq. (3) the $c_{p,HTF}$ is set to $c_{p,HTF} \approx 2.0\ \left[kJ/kg \cdot K\right]$.

For the description of the flow properties at the nozzle, the Reynolds Number ($\mathrm{Re_n}$) by the nozzle diameter has to be calculated by Eq. (20). In Eq. (1) and (2) the temperature dependency from $T_{\alpha,1}$ are taken into account.

$$\mathrm{Re}_n = \frac{\rho_{HTF} \cdot u_{HTF} \cdot D_n}{\eta_{HTF}} \tag{20}$$

with:

$$u_{HTF}(T_{\alpha,1}) = \frac{\dot{m}}{\rho_{HTF}(T_{\alpha,1}) \cdot \pi/4 \cdot D_n^2}$$

leads to: $\mathrm{Re}_n = \dfrac{4 \cdot \dot{m}}{\eta_{HTF} \cdot \pi \cdot D_n^2}$ (21)

3 Results of Experimental Investigation

This paper presents 7 pairs of solidifying and melting experiment runs by the standard procedure in Fig. 4, the parameters of these experiment runs are listed in the *Table 4*.

Table 4: Matrix of experimental parameters

Run_{period} [-]	D_n mm	$\dot{m}$ kg/h	U_n m/s	Re_n [-]	$T_{\alpha,1}$ °C
1_{III}	5	20	0.4	600	-11.6
1_V	5	20	0.4	950	10.9
2_{III}	5	22	0.4	720	-6.5
2_V	5	22	0.4	1040	11.7
3_{III}	5	80	1.4	2500	-7.2
3_V	5	82	1.5	3800	10.6
4_{III}*	5	130	2.4	4250	-7.5
4_V*	5	133	2.5	6120	10.5
5_{III}	5	130	2.4	4100	-7.7
5_V	5	130	2.4	6000	10.7
6_{III}	2	87	10.0	2500	-15.1
6_V	2	87	10.0	4400	15.2
7_{III}	2	110	12.6	3500	-7.5
7_V	2	118	13.6	5450	10.7

*Additional MTMR in the tank, see Fig. 3.

3.1 Temperature Distribution

The temperature distribution is be measured for the period I, III, and V/VI of the experimental procedure. Therefore, the MTMR with 28 TCs, see Fig. 3, is be insured into the tank.

3.1.1 Pre-cooling (Period I)

The temperature distribution of the PCM during the pre-cooling (period I of the experiment procedure) is at the local resolution of the MTMR homogeneous. By neglecting the noise, the temperature of each measuring point in the vertical $T_{PCM,i,3}$ and in horizontal $T_{PCM,i=1.4.7,j}$ are identical, see Fig. 7. In contrast, the temperature distribution of the HTF layer above the PCM has a vertical stratified temperature profile. The temperature differences between the measurement points in the vertical direction $T_{HTF,i,3}$ $(8 \le i \le 11)$ are constant and in horizontal direction $T_{HTF,10,j}$ $(j = 1,2,4,5)$ equal to zero, see Fig. 7.

In contrast to the low temperature spread in the tank, the measured outlet temperature $T_{\omega,2}$ is significant higher. To specify the relevant temperature $T_{\beta,1}$ for the investigation of the heat transfer, there are two

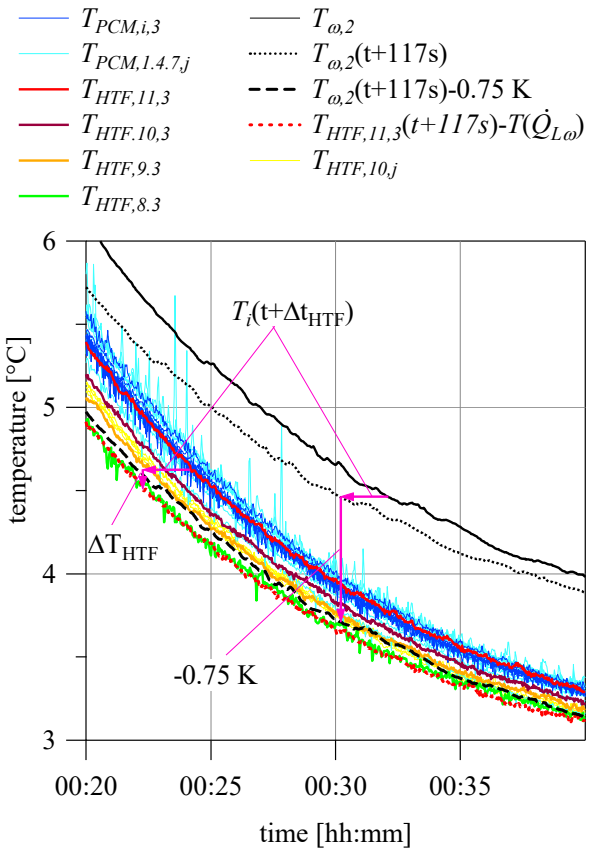

Figure 7*: Measured temperatures from the MTMR during pre-cooling (period I for experiment 4III) of the experimental procedure with an inlet temperature of $T_{\alpha,1} = 2.4°C$ as well as calculated transformation for the outlet temperature with $\Delta t_{HTF} = 117\ s$ and $\Delta T_{HTF} = -0{,}1\ K$.*

possibilities. Both are based on the assumption, that the temperature $T_{HTF,8,3}$ near to the interface PCM-HTF is equal to the outlet temperature of the HTF-droplets ($T_{HTF,8,3} = T_{\beta,1}$). In addition the finding of the stratified temperature profile is used.

On the one hand the temperature $T_{\beta,1}$ is specified by the temperature $T_{HTF,11.3}$ (equal to the temperature at the inlet of the suction tube) and on the other hand by the temperature $T_{\omega,2}$ (temperature measured in the suction tube but outside the tank).

Equation (22) determines the time difference Δt_{HTF}, that a HTF-droplet needs to flow from the PCM-HTF interface to the top of the HTF layer. So, in a first approximation the temperature $T_{HTF,8.3}(t)$ is equal to $T_{HTF,11,3}(t - \Delta t_{HTF})$. Due to the (negative) heat losses of the HTF layer $\dot{Q}_{LH}$, the temperature increases additional. This temperature difference could be calculated by Eq. (23) for a determined $\dot{Q}_{LH}(\Delta\bar{T}_{HTF,A})$.

$$\Delta t_{HTF} = \frac{m_{HTF}}{\dot{m}_{HTF}} \tag{22}$$

$$\Delta T_{HTF} = T_{HTF,8}(t) - T_{HTF,11}(t + \Delta t_{HTF}) = \frac{\dot{Q}_{LH}(\Delta \overline{T}_{HTF,A})}{\dot{m} \cdot c_{p,HTF}(\overline{T}_{HTF})}$$

with: (23)

$$\overline{T}_{HTF} = \frac{T_{HTF,8}(t) + T_{HTF,11}(t)}{2}$$

$$\Delta \overline{T}_{HTF,A} = T_A - \overline{T}_{HTF}$$

Finally, the temperature $T_{\beta,1}$ in dependency to $T_{HTF,11,3}$ could be written as:

$$T_{\beta,1}(t, T_{HTF,11,3}) = T_{HTF,11,3}(t + \Delta t_{HTF}) + \Delta T_{HTF}(\overline{T}_{HTF}) \tag{24}$$

As $T_{HTF,11,3}$ is the temperature at the inlet of the suction tube, the temperature $T_{\beta,1}$ in dependency to $T_{\omega,2}$ has to be calculated in equal terms for the time shift and the heat losses at the tube. However, the heat flow and the heat capacity of the stainless steel tube and the stainless steel jacketed thermal sensor are too complex, to be described in an analytical way. Instead a correction factor of 0.75 K was determined and subtracted from the time shifted measurement. The temperature $T_{\beta,1}$ in dependency to $T_{\omega,2}$ is then calculated by Eq. (25).

$$T_{\beta,1}(t, T_{\omega,2}) = T_{\omega,2}(t + \Delta t_{HTF}) - 0.75\,\mathrm{K} \tag{25}$$

The temperature curves of the calculated values $T_{\beta,1}(t, T_{HTF,11,3})$ and $T_{\beta,1}(t, T_{\omega,2})$ correspond sufficiently to the measured temperature $T_{HTF,8,3}(t)$, see Fig. 7.
The MTMR is inserted to the tank during the experiment runs 4_{III} and 4_{V} only, so the Eq. (25) is used for further investigation, see chapter 3.2.

3.1.2 Solidifying (Period III)

During the solidification of the PCM the measured temperature distribution is not defined, see Fig. 8. Upon completion of the sensitive cooling to T_{melt} a super cooling of 0,3 K is detected before the temperature of the PCM and the HTF layer is constant for about 5 minutes. At the experimental time of 03:00 the outlet temperature $T_{\beta,1}$ of the

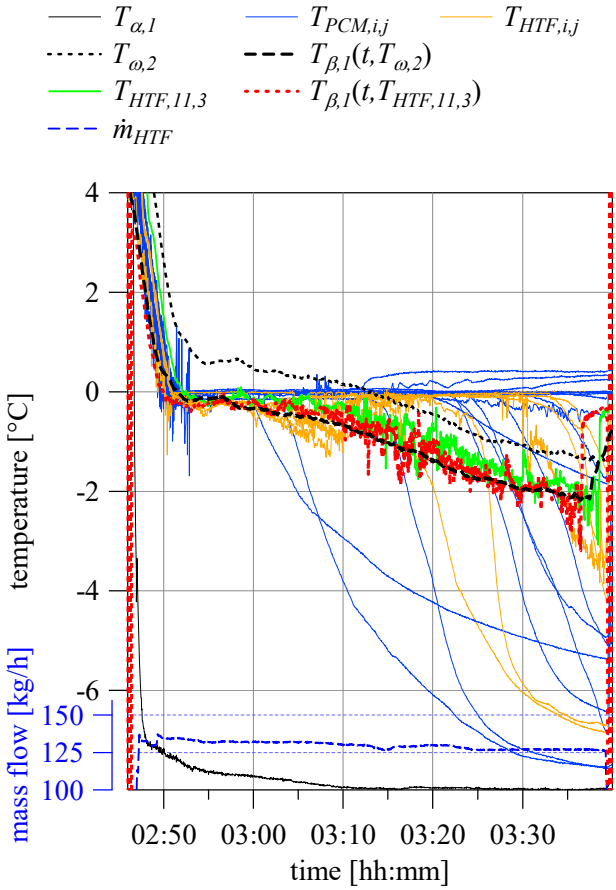

Figure 8: *Measured temperatures from the MTMR during the solidifying ($T_{melt} = 0°C$) of the experimental procedure with an inlet temperature $T_{\alpha,1}$ of -7.5°C (experiment run 4_{III}) as well as calculated translation $T_{\beta,1}(t,T_{\omega,2})$ and $T_{\beta,1}(t,T_{HTF,11})$.*

HTF-droplets begin to decrease slightly and the first temperature curve of a TC in the PCM decrease drastically against the level of inlet temperature $T_{\alpha,1}$.
The drastically decrease of some PCM temperatures is traced back to formed HTF channels. The cold HTF flows through these channels without the high heat transfer rate of a droplet flow. Consequently $T_{\beta,1}$ becomes a mean temperature of cold HTF out of the channels (low heat transfer rate at the channel walls) and the HTF is heated up by the droplet flow against T_{melt} (high heat transfer rate), therefor the temperature $T_{\beta,1}$ decrease.
At 03:10 two phenomena start: some temperatures of the TC in the PCM increase against 0.4°C and the temperature of the most TC in the HTF increases to $T_{melt} = 0°C$.
The increasing of some PCM temperatures are detected in the lowest horizontal measurement line ($T_{PCM,1,j}$). In this area during all experiment runs

a phase change never was detected. In addition, the velocity of the PCM_l could neglected because a wall of solidified PCM_s separate the HTF-flow from the PCM_l. One possible explanation may be the heat losses of the LED-panels (installed at the tank wall) heat the PCM. However, the measurement of the heat losses $\dot{Q}_{LP}$ included this energy flow already, so that is does not influence to the investigation of the heat transfer.

The increasing of most of the HTF temperatures takes into account the density change over the phase change which is supported by encapsulation of HTF droplets in the PCM_s matrix. Due to a density change, the high of the interface increase over the horizontal measurement line ($T_{HTF,4,j}$) so that it is covered by PCM.

A comparison of $T_{\beta,1}(t,T_{\omega,2})$ and $T_{\beta,1}(t,T_{HTF,11})$ shows that both calculating methods results in similar temperatures. Due to the lower noise of $T_{\omega,2}$ in comparison to $T_{HTF,11}$ the calculated values by $T_{\beta,1}(t,T_{\omega,2})$ also show a lower noise than those calculated by $T_{\beta,1}(t,T_{HTF,11})$.

The increase of $T_{\beta,1}$ at 03:37 is due to the time shift by Δt_{HTF} and the increase of the measured temperatures $T_{\omega,2}$ and $T_{HTF,11}$ during the period IV. The red dotted walls at the beginning and the end of the diagram represent periods II (beginning) and IV (end).

3.1.3 Melting (Period V)

As well as during the solidifying, the temperature distribution during the melting of the PCM is not definite, see Fig. 9. Directly from the start of the period V on, the temperatures of the PCM increase and the temperatures of the HTF stay constant at $T_{melt} = 0°C$. While most of the measured PCM temperatures increase nearly linear with 0.2 K/min in the first 40 minutes, the temperatures for $T_{\beta,1}$ form after 10 minutes a temperature plateau around 2°C for 15 minutes. After the plateau the temperatures increase as well with 0.2 K/min.

PCM temperatures that do not increase from the beginning but start later, increase linear as well but with a higher rate until they reach the temperature level of the other PCM temperatures. By observation through the glass plate, this development could be explained by the different flow regimes at the TCs. A TC in the main and turbulent flow regime is melting free rapidly in comparison to a TC that is in a low turbulent flow regime. The already free-melted TCs

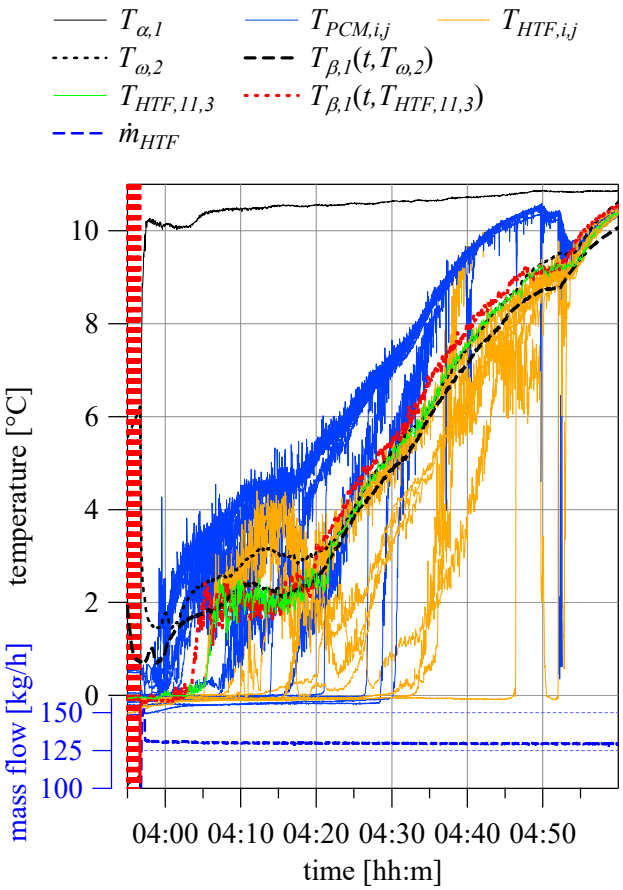

Figure 9: *Measured temperatures from the MTMR during melting (T_{melt} = 0°C) of the experimental procedure with an inlet temperature of $T_{\alpha,1}$ = 10.5°C (experiment run 4_V) as well as calculated temperature transformation $T_{\beta,1}(t,T_{\omega,2})$ and $T_{\beta,1}(t,T_{HTF,11})$.*

show the same temperature, so the temperature distribution of the PCM_l is homogenous with exception the PCM_l in the channels.

The development of the measured HTF temperatures is roughly identical. There are, however, two quantitative differences. First, the increase of the temperatures starts later and second, the homogeneous temperature level at the free-melted TC is lower. Optical observations point out, that the PCM_s needs more time for melting, if it placed in the low turbulent HTF level instead in the high turbulent PCM_l level. Due to the high turbulence, initiated by the droplet flow, the heat transfer rate in the PCM_l level is significant higher than in the HTF level.

At the experimental time 04:50 the PCM temperatures decrease rapidly to the level of the HTF and afterwards all temperatures increase identically. A possible explanation for this phenomenon is that a

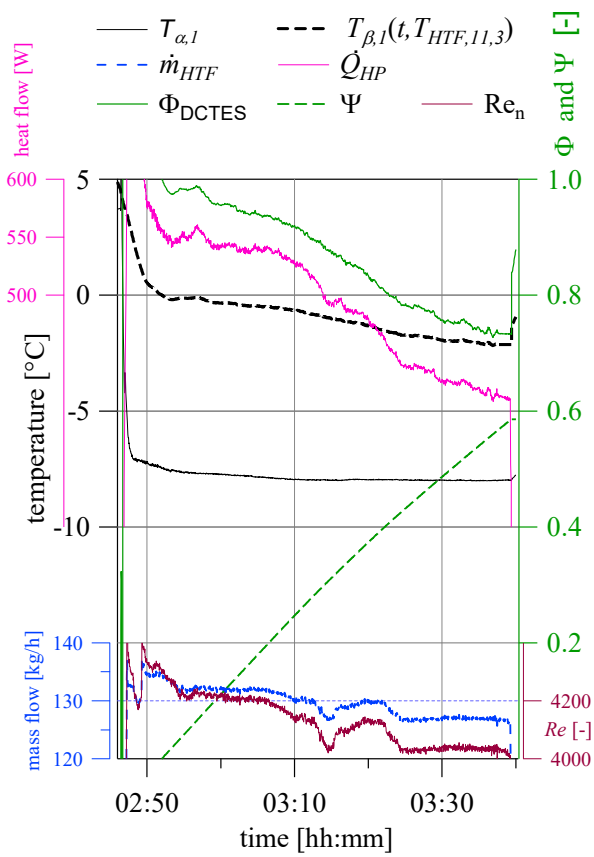

Figure 10: *Measured inlet temperature $T_{\alpha,1}$ and mass flow $\dot{m}_{HTF}$ and calculated values of the experiment run 4_{III}.*

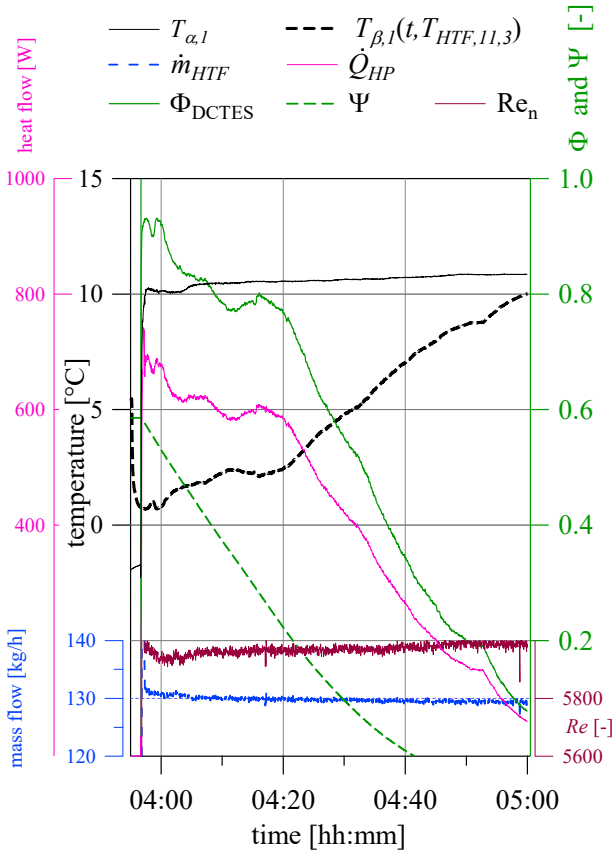

Figure 11: *Measured inlet temperature $T_{\alpha,1}$ and mass flow $\dot{m}_{HTF}$ and calculated values of the experiment run 4_V.*

agglomeration of PCM_s lose his contact to a constructive storage compound and sink from the HTF into the PCM_l level. There it melts rapidly because of the warm and turbulent PCM_l flow, whereby the PCM temperatures decrease.

The two values for $T_{\beta,1}$ are identical only on the temperature plateau of 2°C. Before the plateau the temperature of $T_{\beta,1}(t,T_{\omega,2})$ is up to 1.5 K higher. By the (negative) heat losses during period IV (with no HTF flow), tube and sensor of $T_{\omega,2}$ reach 6°C. This influences the measurement at the beginning of the period V. After the plateau $T_{\beta,1}(t,T_{\omega,2})$ is constantly 0.5 K lower than $T_{\beta,1}(t,T_{HTF,11})$. This may be explained by the constant temperature correction factor of 0.75 K in Eq. (25), which was determined for a temperature level of T_{melt}. Instead, the temperature level is up to 9 K above T_{melt}, so that the (negative) heat losses to the ambient are lower and the correction factor is too high.

3.2 Time Based Thermodynamic Evaluation

The thermodynamic evaluation in detail is presented by taking experiment runs 4_{III} and 4_V as example. In addition to the non-dimensions parameters Φ_{DCTES} (Eq. 14) and Ψ (Eq. 15), the curve of the heat flow $\dot{Q}_{HP}$ is plotted in the diagrams of Fig. 10 and Fig. 11 as well. The comparison of the curves of Φ_{DCTES} and $\dot{Q}_{HP}$ demonstrates the suitability of Φ_{DCTES} to describe the performance of $\dot{Q}_{HP}$, see Fig. 10 and Fig. 11. For the suitability of Ψ to describe the latent stored energy the evidence is be renounced in respect to the clarity of the diagrams.

Fig. 10 shows the behavior of the relevant measurements and calculated values for the thermodynamic evaluation for the solidification process (experiment run 4_{III}) and Fig. 11 of the melting process (experiment run 4_{IV}).

In both experiment runs $\dot{m}_{HTF}$ was 130 kg/h although the mass flow is fluctuating during the solidification process. The turbulence at the nozzle Re_n corresponds primarily to the mass flow. But due to the higher level of $\overline{T}_{HTF}$ and dependent on the

material properties to the temperature, Re_n during the melting process is about 50% higher than during the solidification.

The temperature curves of $T_{\alpha,1}$ and $T_{\beta,1}$ are described in detail in chapter 3.1.

The mass ratio of solidified PCM Ψ increases nearly linear with a mean gradient of 0.7 h^{-1} but in detail, the gradient decreases over the time. During the melting process $\Psi = 0$ (PCM is completely molten) is reached at the experiment time of 04:40, although the curve of $T_{\beta,1}$ and optical observation indicate, that the melting process is not finished. The end of the melting process was determined in chapter 3.1.2 to the experimental time of 04:50. A necessary assumption to use the Eq. (15) for Ψ is that there is no sensitive heating of the PCM_l and PCM_s during the phase change. As seen in Fig. 9 the temperature of the PCM_l is not constant, in consequence Ψ may not be calculated by Eq. (15).

The curve of Φ_{DCTES} decreases over the time. During solidification the curve could be interpreted as linear with a mean gradient of -0.4 h^{-1}. Opposed to this, during the melting process the curve separates two parts. The first part is from 04:00 to 04:20 shows a mean gradient of 0.3 h^{-1} and the second part from 04:20 to 04:50 shows a mean gradient of 1 h^{-1}. The reason for the prompt change of the gradients is not known at the moment.

The curves of $\dot{Q}_{HP}$ at both phase change processes have the same manner as the curves of Φ_{DCTES}. However, during the solidification the curve of $\dot{Q}_{HP}$ shows additional fluctuations based on the fluctuations of $\dot{m}_{HTF}$.

3.3 Non Dimension Thermodynamic Evaluation

It may be assumed that the heat transfer between the HTF and the PCM is dependent on the state of the solidified PCM. The state of the PCM_s could, for example, described by the porosity or mode of the distribution in the tank. However, the only information about the state of the PCM_s derived from the measurements is the mass ratio Ψ for the solidification process. On the other hand, the heat efficiency Φ_{DCTES} characterizes the quality of heat transfer.

Figure 12 shows Φ_{DCTES} all the solidification experiments concerning Ψ. Out of practical reasons the experiments had not reach a complete solidified state. By that, the maximal range of values for Ψ is $0 \leq \Psi \leq 0.9$. For Φ, the values above 1.0 are not be interpreted here.

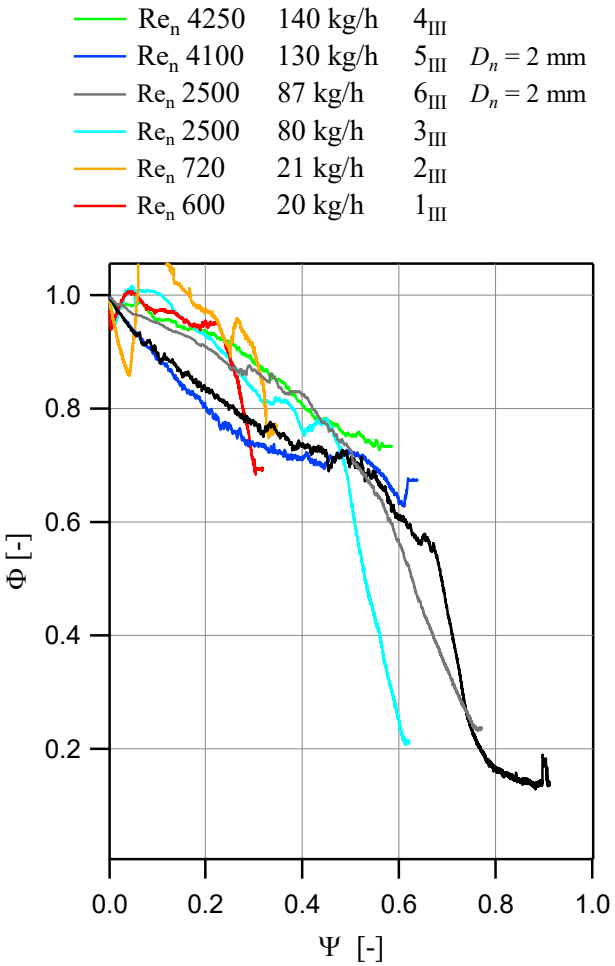

Figure 12: The heat effectiveness Φ_{DCTES} over the mass ratio Ψ of the solidification process from the experiment runs 1 to 7.

The curves show two characteristic attributes of the heat transfer behaviour over the mass ratio Ψ.

One characteristic is that all curves with Re_n greater than 720 go near to the point $\Phi_{DCTES}(\Psi = 0.5) \approx 0.7$.

The experiments 1_{III} and 2_{III} finish at $\Psi \approx 0.3$, so it could not attest, if there curves will also match the point at $\Psi = 0.5$.

The second characteristic is that the curves 1_{III}, 2_{III}, 3_{III} and 7_{III} show a definite point, where the amount of the gradient increases instantly. One approach to assume a correlation for the edge in the curve is that the value of Ψ at the edge increases if Re_n increases. The number of curves is too small to confirm or quantify this assumption of a correlation. In addition the curves show a local minimum before the edge that could not explained. The experiment 6_{III} shows a change in the value of the gradient in the same order as in the other curves, but the change of the gradient is more constant, so that there is no edge in the curve.

4 Conclusion

The measurement of the temperature distribution confirm, that the conversion from $T_{\omega,2}$ to $T_{\beta,1}(t,T_{\omega,2})$ is valid. Although only in one experiment the MTMR in the tank validates the conversion, the values are plausible and coherent.

The decrease of the curve of $T_{\beta,1}(t,T_{\omega,2})$ over the time during the solidification is based on the increasing amount of channels with a pure HTF flow inside. The heat transfer rate inside these channels is lower than in a droplet flow, so that heat flow and thus the temperature of $T_{\beta,1}(t,T_{\omega,2})$ decrease.

The characteristic of the temperature distribution during the melting process is the result of a mixture of latent and sensible storage properties. Subsequently these measurements could point to the assumption that by DCTES a stable temperature plateau with a constant power can be reached for the solidification process, but not for the melting. This assumption is not strongly grounded, because it is based on one nozzle configuration with one combination of PCM and HTF only. The temperature profile by the melting process has to be investigated intensively, in order to reach a balanced performance between the solidification and melting processes.

The time based thermodynamic evaluation confirmed the informative value of the non-dimensional values Φ_{DCTES} and Ψ for the solidification process. Though the equation for Ψ is not valid for the melting process, Φ_{DCTES} is still valid. If a equation to calculate Ψ out of the measurement data could be found, the non-dimension thermodynamic evaluation could be extended to the melting process as well.

The non-dimension evaluation of the solidification process indicates correlations between the $\mathrm{Re_n}$ and the characteristics of the curves from Φ_{DCTES}. The data set is too incomprehensive to formulate the correlation in detail. However, it is promising to find correlations for the gradient before the edge of the curve and the value of Ψ. Thus changes on the storage construction can be assessed and skipped to construction guidelines.

5 Outlook

The measurement of the temperature distribution in the tank helps to understand the characteristics of temperature performance although the MTMR influences the flow field. To indicate the influence of $\dot{m}$ and $\mathrm{Re_n}$ on the phase change processes in detail, the measurements have to be performed with a wider range of mass flows. Additionally the analysis of the data have to be extended by a time and local resolved method.

The non-dimensionless evaluation is a powerful tool to assess the storage performance. To indicate and quantify correlation of constructional or material influences on the performance properties of the storage, a more extensive database is necessary. Therefore, each experiment should reach the state of a complete solidified storage ($\Psi = 1$) and verified by a minimum of one repetition. To reduce the experimental effort, the reproducibility should be examined in detail for single configuration. The measurement on the experimental set-up works well, but the position of the sensor for $T_{\omega,2}$ has to be decoupled from the heat flow caused by the environment. Due to a thinner sensor and a measurement position directly at the inlet of the surge tube, the influences of constructional based heat flows could reduce.

Finally, optical investigation has a promising potential to support the understanding of the state of the phase change processes. To use optical investigation in an efficient way, significant information derived from pictures has to be transformed into numerical values in an automated procedure.

6 Acknowledgment

This research was supported by the Swiss National Science Foundation (SNSF, project number PZENP2_173636) and the Swiss Competence Center for Energy Research Storage of Heat and Electricity (SCCER HaE, contract No. 155002545).

7 Nomenclature

c_p	specific heat capacity
D_n	nozzle Diameter
h	specific enthalpy
$\dot{H}$	enthalpy flow
$m, \dot{m}$	mass, mass flow
$Q, \dot{Q}$	energy, heat flow
t	time
T	temperature
η	dynamic viscosity
λ	heat conduction
ρ	density
Φ	temperature effectivity
Ψ	mass ratio of solidified PCM
$\mathrm{Re_n}$	Reynolds number

References:

[1] A. Arteconi, N.J. Hewitt, F. Polonara, Domestic demand-side management (DSM): Role of heat pumps and thermal energy storage (TES) systems, Appl. Therm. Eng. 51 (2013) 155–165. doi:10.1016/j.applthermaleng.2012.09.023.

[2] K. Merlin, J. Soto, D. Delaunay, L. Traonvouez, Industrial waste heat recovery using an enhanced conductivity latent heat thermal energy storage, (2016). doi:10.1016/j.apenergy.2016.09.007.

[3] G. Alva, Y. Lin, G. Fang, An overview of thermal energy storage systems, Energy. 144 (2018) 341–378. doi:10.1016/j.energy.2017.12.037.

[4] H. Pointner, W.D. Steinmann, M. Eck, C. Bachelier, Separation of Power and Capacity in Latent Heat Energy Storage, Energy Procedia. 69 (2015) 997–1005. doi:10.1016/j.egypro.2015.03.189.

[5] M.M. Farid, A.M. Khudhair, S.A.K. Razack, S. Al-Hallaj, A review on phase change energy storage: materials and applications, Energy Convers. Manag. 45 (2004) 1597–1615. doi:10.1016/j.enconman.2003.09.015.

[6] K. Pielichowska, K. Pielichowski, Phase change materials for thermal energy storage, Prog. Mater. Sci. 65 (2014) 67–123. doi:http://dx.doi.org/10.1016/j.pmatsci.2014.03.005.

[7] S.S. Chandel, T. Agarwal, Review of current state of research on energy storage, toxicity, health hazards and commercialization of phase changing materials, Renew. Sustain. Energy Rev. 67 (2017) 581–596. doi:10.1016/j.rser.2016.09.070.

[8] J. Pereira da Cunha, P. Eames, Thermal energy storage for low and medium temperature applications using phase change materials – A review, Appl. Energy. 177 (2016) 227–238. doi:10.1016/j.apenergy.2016.05.097.

[9] M. Delgado, A. Lázaro, C. Peñalosa, B. Zalba, Experimental analysis of the influence of microcapsule mass fraction on the thermal and rheological behavior of a PCM slurry, Appl. Therm. Eng. 63 (2014) 11–22. doi:10.1016/j.applthermaleng.2013.10.011.

[10] J. Shao, J. Darkwa, G. Kokogiannakis, Development of a novel phase change material emulsion for cooling systems, Renew. Energy. 87 (2016) 509–516. doi:10.1016/j.renene.2015.10.050.

[11] R. Velraj, R.V. Seeniraj, B. Hafner, C. Faber, K. Schwarzer, Heat Transfer Enhancement in a Latent Heat Storage System, Sol. Energy. 65 (1999) 171–180. doi:10.1016/S0038-092X(98)00128-5.

[12] S. Jegadheeswaran, S.D. Pohekar, Performance enhancement in latent heat thermal storage system: a review, Renew. Sustain. Energy Rev. 13 (2009) 2225–2244.

[13] Y. Yuan, X. Cao, B. Xiang, Y. Du, Effect of installation angle of fins on melting characteristics of annular unit for latent heat thermal energy storage, Sol. Energy. 136 (2016) 365–378. doi:10.1016/j.solener.2016.07.014.

[14] S.D. Sharma, K. Sagara, Latent Heat Storage Materials and Systems: A Review, Int. J. Green Energy. 2 (2005) 1–56. doi:10.1081/GE-200051299.

[15] T. Nomura, M. Tsubota, T. Oya, N. Okinaka, T. Akiyama, Heat storage in direct-contact heat exchanger with phase change material, Appl. Therm. Eng. 50 (2013) 26–34. doi:10.1016/j.applthermaleng.2012.04.062.

[16] T. Nomura, M. Tsubota, N. Okinaka, T. Akiyama, Improvement on Heat Release Performance of Direct-contact Heat Exchanger Using Phase Change Material for Recovery of Low Temperature Exhaust Heat, ISIJ Int. 55 (2015) 441–447. doi:10.2355/isijinternational.55.441.

[17] Y. Wang, L. Wang, N. Xie, X. Lin, H. Chen, Experimental study on the melting and solidification behavior of erythritol in a vertical shell-and-tube latent heat thermal storage unit, Int. J. Heat Mass Transf. 99 (2016) 770–781. doi:10.1016/j.ijheatmasstransfer.2016.03.125.

[18] W. Wang, H. Li, S. Guo, S. He, J. Ding, J. Yan, J. Yang, Numerical simulation study on discharging process of the direct-contact phase change energy storage system, Appl. Energy. 150 (2015) 61–68. doi:10.1016/j.apenergy.2015.03.108.

[19] S. Guo, J. Zhao, W. Wang, G. Jin, X. Wang, Q. An, W. Gao, Experimental study on solving the blocking for the direct contact mobilized thermal energy storage container, Appl. Therm. Eng. 78 (2015) 556–564. doi:http://dx.doi.org/10.1016/j.applthermaleng.2014.12.008.

[20] H. Nogami, K. Ikeuchi, K. Sato, Fundamental Flow Characteristics in a Small Columnar Latent Heat Storage Bath, ISIJ Int. 50 (2010) 1270–1275. doi:10.2355/isijinternational.50.1270.

[21] X.Y. Li, D.Q. Qu, L. Yang, K. Di Li, Experimental and numerical investigation of discharging process of direct contact thermal energy storage for use in conventional air-

conditioning systems, Appl. Energy. 189 (2017) 211–220. doi:10.1016/j.apenergy.2016.11.094.
[22] J. Xu, Q. Xiao, Y. Fei, S. Wang, J. Huang, Accurate estimation of mixing time in a direct contact boiling heat transfer process using statistical methods, Int. Commun. Heat Mass Transf. 75 (2016) 162–168. doi:10.1016/j.icheatmasstransfer.2016.04.012.
[23] E. Almeras, V. Mathai, D. Lohse, C. Sun, Experimental investigation of the turbulence induced by a bubble swarm rising within an incident turbulence, (2017) 1091–1112. doi:10.1017/jfm.2017.410.
[24] D. Pjontek, J. Landry, C.A. McKnight, L.P. Hackman, A. Macchi, Effect of a dispersed immiscible liquid phase on the hydrodynamics of a bubble column and ebullated bed, Chem. Eng. Sci. 66 (2011) 2224–2231.
[25] B.C. Hermann, Weingärtner; Franck, Ernst Ulrich; Wiegand, Gabriele; Dahmen, Nicolaus; Schwedt, Georg; Frimmel, Fritz H.; Gordalla, Water, 1. Properties, Analysis and Hydrological Cycle, in: Ullmann's Encycl. Ind. Chem., Vol. 39, Wiley-VCH Verlag GmbH & Co. KGaA, Weinheim, 2012: pp. 1–40. doi:10.1002/14356007.a28_001.pub2.
[26] FRAGOL GmbH+Co. KG, Wärmeträgerflüssigkeiten, (2017) 60.